$Sr\_14Cu\_24O\_41$: a complete model for the chain sub-system

Marie-Bernadette Lepetit, Alain Gellé

$Sr_{14}Cu_{24}O_{41}$: a complete model for the chain sub-system

Alain Gellé, Marie-Bernadette Lepetit
Laboratoire de Physique Quantique, IRSAMC / UMR 5626, Université Paul Sabatier, 118 route de Narbonne, F-31062 Toulouse Cedex 4, FRANCE
(Dated: October 8, 2004)

A second neighbor $t-J+V$ model for the chain subsystem of the $Sr_{14}Cu_{24}O_{41}$ has been extracted from ab-initio calculations. This model does not use periodic approximation but describes the entire chain through the use of the four-dimensional crystallographic description. The link between the parameters variations and the structural distortions have been discussed. This model allowed us to understand the origin of the chain dimerization and predicts correctly the relative occurrence of dimers and free spins. The orbitals respectively supporting the magnetic electrons and the holes have been found to be essentially supported by the copper $3d$ orbitals (spins) and the surrounding oxygen $2p$ orbitals (holes), thus giving a strong footing to the existence of Zhang-Rice singlets.

PACS numbers: 71.10.Fd, 71.27.+a, 71.23.Ft

I. INTRODUCTION

One-dimensional quantum systems have attracted a lot of attention in the past decade due to the large diversity of their low energy physics. In particular, spin-chains and spin-ladders systems have been extensively studied. The characteristic of the $Sr_{14-x}A_xCu_{24}O_{41}$ ($A = Ca, Ba, Y, Bi$, etc.) family of transition-metal oxides is that they are composed of both spin-chains and spin-ladders sub-systems. The compounds are formed of alternated layers (in the (a,c) plane) of each of the two subsystems[1]. Both ladder and chains are in the $\mathbf{c}$ direction. However their respective translation vectors ($\mathbf{c_c}$ and $\mathbf{c_l}$) are incommensurate. In the pure compound, $Sr_{14}Cu_{24}O_{41}$, the layers are largely separated ($\simeq 3.3$Å) and considered as electronically non interacting. Nevertheless, the low energy properties of $Sr_{14}Cu_{24}O_{41}$ agree neither with those of spin-chains, nor with the properties of spin-ladders.

$Sr_{14}Cu_{24}O_{41}$ is a semiconductor with a 0.18 eV gap[2] at $T < T^\star = 250K$. The spin ladders have a singlet ground state with a spin gap of about $35-47$ meV[3,4,5]. Surprisingly the spin chains also exhibit a singlet ground state with a spin gap of $11-12\,meV$[2,5,6,7,8] while homogeneous spin chains are known to be gap-less in the spin-channel. Susceptibility and ESR measurement[2,9] suggested that the spin gap in the chains is due to the formation of weakly interacting spin dimers. Neutron scattering experiments[3] have latter confirmed their existence.

The spins are supported in the chain subsystem by the $3d_{ac}$ orbitals of the Cu^{2+} ions, and in the ladder subsystem by the $3d_{a^2-c^2}$ orbitals of the Cu^{2+} ions. In the chain subsystem the magnetic orbitals are coupled via two nearly 90° *Cu–O–Cu* bonds. Let us note at this point that, in such geometries, the super-exchange paths through the oxygen orbitals interact destructively and therefore nearest-neighbor (NN) exchange interactions are expected to be small and ferromagnetic. In the ladder subsystem, the picture of the NN interactions is very different since there are mediated via nearly 180° *Cu–O–Cu* angles. Such geometries are known to produce strong super-exchange mechanism via the bridging ligands and thus large anti-ferromagnetic interactions.

Formal charge analysis shows that the $Sr_{14}Cu_{24}O_{41}$ compound is intrinsically doped with six holes by formula unit (f.u.). Similar to high-T_c superconductors, the holes were expected to be mainly supported by the oxygen $2p$ orbitals and to form Zhang-Rice[10] singlets with the associated-copper hole. NEXAFS (Near Edge Xray Absorption Fine Structure) experiments[11] have later supported this assumption.

It has been established, from neutron scattering[3] and X ray spectroscopy[12] experiments, that the chain dimeric units are formed by next-nearest-neighbor (NNN) spins separated by a Zhang-Rice singlet (ZRS). *Cu* NMR measurements exhibited the presence of two kinds of ZRS on the chains[4], namely with intra- and inter-dimer localization. The relative occurrence of the two types of ZRS ($0.65 \simeq 1/2$) led the authors to propose a charge-order model with dimers separated by two ZRS. This assumption has been confirmed by neutron scattering experiments[7,13] that have shown to be consistent with a five units periodicity. Such a picture leads to a chain filling of 6 holes per f.u., that is with all the holes located on the chains. The question of the holes repartition between the chain and ladder subsystems is however still under debate. Indeed, NEXAFS experiments[11] evaluated to 0.8 the number of holes on the ladders legs oxygens. On the contrary, magnetic susceptibility measurements[2] exhibit a filling of 3.5 spins per f.u., that is 0.5 more holes than the maximum number given by the formal charge analysis.

The origin of the chain electronic dimerization has only recently being elucidated. The hypothesis of a spin-Peierls transition have been rapidly eliminated since the expected signatures in the magnetic susceptibility and specific heat were not found. It thus has long been supposed that the dimerization originated from the competition between first and second-neighbor spin interactions as predicted by Majumdar and Gosh[14] and Haldane[15]. Recent ab initio calculations[16] have however shown that the origin of the dimerized state is of structural origin,

even if not of spin-Peierls one. Indeed, this is the structural incommensurate modulation of the chain subsystem, with the periodicity of the ladder one, that strongly modulates the spin/hole orbital energy and localizes the spins in a dimer pattern.

These incommensurate structural modulations, that are most of the time neglected, have thus proved to be crucial for the low energy properties of this system. Independently to the orbital energy modulations, the structural distortions of the chain subsystem can be expected to strongly influence both effective exchange and hopping integrals. The present work thus aims at giving a complete description of the chain subsystem within a second neighbor $t-J+V$ model, taking explicitly into account the structural incommensurate modulations. The incommensurate character of the problem will be treated within the four-dimensional representation and we will describe the electronic structure without the use of a periodic approximation. The next section will describe the ab-initio methods used in the present calculations. Section III will present ab-initio evidence of the Zhang-Rice singlets. Section IV will give the second neighbor $t-J+V$ model as a function of the fourth crystallographic coordinate τ. Section V will detail the filling analysis resulting from the proposed model. Finally section VI will focus on the conclusion.

II. THE AB-INITIO METHOD

It is well known that magnetic and transfer interactions are essentially local in strongly correlated systems and can thus be accurately evaluated using embedded fragment ab-initio spectroscopy methods[17]. The long range electrostatic effects are treated within a bath composed of total-ion pseudo-potentials[18] and charges. The open-shell character of the magnetic/hole orbitals, the strong electronic correlation as well as the screening effects are efficiently treated using quantum-chemistry ab-initio spectroscopy methods. The present calculations have been performed using the Difference-Dedicated Configuration Interaction method[19] that have proved to be very efficient on copper and vanadium compounds such as high T_c copper oxides[20] or the famous $\alpha' NaV_2O_5$ compound[21].

The quantum fragments are defined so that to include (i) the magnetic centers, (ii) the bridging oxygens mediating the interactions, and (iii) the first coordination shell of the preceding atoms which is responsible for the essential part of the screening effects. First neighbor interactions are thus determined using Cu_2O_6 fragments (see figure 1a), while second-neighbor ones are computed using Cu_3O_8 fragments (see figure 1b). NN exchange, J_1, is directly given by the singlet-triplet excitation energy when two magnetic electrons are considered in the small fragment. NN hopping, t_1, and magnetic electron/hole orbital energy differences $\delta\varepsilon$ are extracted from the first two doublet states of the same fragment with one electron less. NNN exchange interactions J_2 are extracted from the doublet-quartet excitations energies from the three-centers fragment with 3 magnetic electrons. NNN hopping and first neighbor bi-electronic Coulomb repulsion are obtained from the 3 singlets and 3 triplets of same fragment with one magnetic electron less. Let us point out that the 3 centers calculations also yield the NN interactions. The comparison between the evaluations of the first-neighbor integrals obtained from the 2 centers and 3 centers fragments allows us to verify the relevance of the chosen model and the fragment size dependence of our calculations. A least-square fit method is used in order to extract the effective parameters from the ab-initio calculations. The conditions imposed for this purpose are that the effective model should reproduce

- the computed excitations energies,
- the projection of the computed wave-functions within the configuration space generated by the magnetic orbitals.

Let us note that the norm of the later projection gives us a measure of the model validity. Indeed, the ab-initio wave-functions (which is expanded over several millions of configurations) projects over the model configuration space based only on the magnetic orbitals (typically of the order of 10 configurations) with a norm as large as 0.8. One can thus assume that this model space is appropriate to describe the low energy physics of the system.

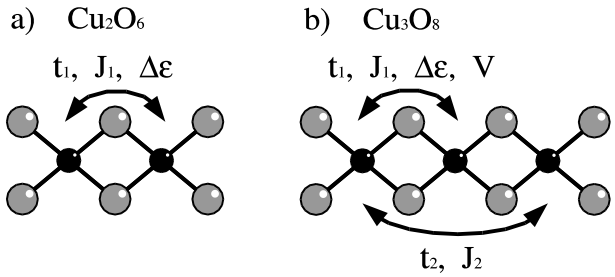

FIG. 1: a) Schematic representation of the computed fragments. a) two centers b) three centers. The gray circles represent oxygen atoms, while the black circles represent the copper atoms.

Let us now address the embedding problem for incommensurate systems. The usual embedding technique consists of reproducing the Madelung potential using a set of point charges, located at the crystallographic positions over a box of at least 15 to 20 Å around the fragment[22]. These charges are adjusted on the bath borders according to an Evjen procedure[23]. In the case of a periodic ionic crystal this method insures the nullity of both the system charge and dipole moment, both conditions are necessary to insure a good representation of the Madelung potential. In the present incommensurate case, however, the Evjen procedure fails to suppress the dipole moment.

This is due to the fact that the chain and ladder subsystems are not electrostatically neutral. The relative displacement of one compared to the other thus induces a dipole moment in the chain/ladder direction. In order to solve this problem, and to cancel out the dipole moment contribution, we adjusted the charges of the outermost unit cells of each subsystem, in the c direction, using a global scaling factor for each adjusted cell[24].

The type of calculations have been done on 11 equivalent fragments located at 11 successive positions in the chain direction. These 11 fragments give a quite good representation of the different distortions occurring on the chain subsystem. In order to fully represent the whole chain subsystem, these 11 sets of results have been extrapolated, using Fourier's series analysis, as a function of the crystallographic fourth coordinate τ, associated with the system incommensurate modulations.

Let us notice that in a complete crystallographic description[25], each atom possesses a fourth fractional coordinate $\tau_i = \mathbf{r_i} \cdot \mathbf{k} = z_i c_c/c_l$, where $\mathbf{r_i}$ is the atom position, $\mathbf{k} = \mathbf{c_c^\star} c_c/c_l$ is the modulation vector, z_i is the fractional coordinate of the atom in the $\mathbf{c}$ direction. In the model Hamiltonian used in present work, τ corresponds to the fourth coordinate of the chain unit-cell copper atom. It is defined except for a constant.

III. THE ZHANG-RICE SINGLETS

As previously noticed, it has been supposed in the literature that the holes (both in the chain and ladder subsystems) are not located on the copper atoms but rather on the surrounding oxygens. This assumption has been done by analogy with the high T_c copper oxides and has later been comforted by NEXAFS experiments[11] as far as ladder holes are concerned. We have thus derived from our ab-initio calculations the nature and composition of both the magnetic (supporting the spins) and hole orbitals.

The magnetic orbitals have been obtained, from the 2 centers fragment calculations, as the triplet natural orbitals (eigenfunctions of the one-electron density matrix) with an occupation number close to 1. In order to locate the hole orbitals we compared two calculations on the same fragment with one electron difference. The hole orbitals have been extracted from the difference between twice the triplet density-matrix and the sum of the two doublet ones. The hole orbitals are thus the two eigenfunctions of the resulting matrix associated with eigenvalues close to 1.

Figure 2 represents a typical example of both the magnetic (a) and hole (b) orbitals on a site. It clearly appears that while the magnetic orbital is essentially supported by the $3d_{ac}$ copper orbital with a delocalization tail on the surrounding $2p$ oxygens orbitals, the hole orbital is essentially supported by the $2p$ oxygen orbitals with a small tail on the $3d_{ac}$ orbital of the copper atom. The average repartition between copper and oxygens — over the 11 calculations — are as follow :

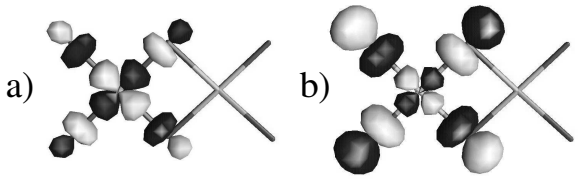

FIG. 2: a) Example of magnetic orbital supporting the spin, b) associated hole orbital.

- for the magnetic orbital : 67% on the copper and 33% on the oxygens,
- for the hole orbital : 15% on the copper and 85% on the oxygens.

The fluctuation of the above repartition on the 11 computed fragments is very small with a standard deviation of only 1.3%.

The present results showing the existence of different orbitals, respectively supporting the spins and the holes, constitute a direct evidence of the ZR singlets in the system.

IV. THE $t - J + V$ MODEL

The model Hamiltonian describing physics of the chain subsystem has been chosen as currently accepted in the literature, that is as a second-neighbor $t - J + V$ model. Let us recall the justifications of this model.

- The strongly correlated character of the $3d$ copper orbitals, as well as the low filling of the system, justify the exclusion of an explicit reference to the configurations where the magnetic orbitals are doubly occupied, and thus a $t-J$ type of Hamiltonian.
- The nearly 90° *Cu–O–Cu* angle is responsible for weak first neighbor interactions. Second neighbor interactions are thus competitive with the NN ones and must be taken explicitly into account.

The computed results have been fitted, as a function of the fourth crystallographic coordinate τ, using a Fourier series, according to the following expression

$$a_0 + \sum_n a_n \cos\left(2\pi n\tau - \varphi_n\right) \qquad (1)$$

Only terms with a non negligible contribution to the series have been retained. It results that the orbital energies, hopping integrals and NN repulsion terms can accurately be obtained from a unique cosine. Exchange integrals, however, necessitate two components to be reliably reproduced, as can be expected from the quadratic dependence of the latter to the hopping integrals.

The results are summarized in table I. Let us notice that only terms with even frequencies have a non negligible contribution ($n = 2$ and $n = 4$ in eq. 1). This can be interpreted as a doubling of the modulation vector $\mathbf{k}$. The fourth coordinate of a unit cell is thus given by

$$\tau = z \times 2\, c_c/c_l \simeq z \times 2 \times 7/10$$

where z is the fractional coordinate in the $\mathbf{c}$ direction of the unit cell copper atom. It thus clearly appears that the model Hamiltonian presents a 5 unit cell quasi-periodicity. This point is in agreement with the neutron scattering experiments[7,13] that sees a pseudo periodicity of the spin arrangement corresponding to five chain unit cells.

	ε (eV)	V (eV)	t_1 (meV)	t_2 (meV)	J_1 (meV)	J_2 (meV)
a_0	0	0.661	132.0	214.3	20.88	−6.81
a_2	0.600	−0.063	−67.2	−45.3	−2.63	1.80
φ_2	0	−0.353	−0.401	−0.442	−0.329	−0.450
a_4				4.2	−2.29	0.26
φ_4				0.521	−0.411	−0.368

TABLE I: Analytic fit of the $t-J+V$ second neighbor model.

A. The orbital energies

Figure 3 displays the orbital energy differences between two neighboring sites as a function of τ as well as the hole orbital energies deduced from them. One sees immediately that the orbital energy modulations are very large and spans a 1.2 eV range. In fact, these variations are larger (see table I) than any of the other parameters of the system, exept for the NN electron-electron repulsion. As we already showed in reference[16] this parameter is responsible for the electron localization and ordering.

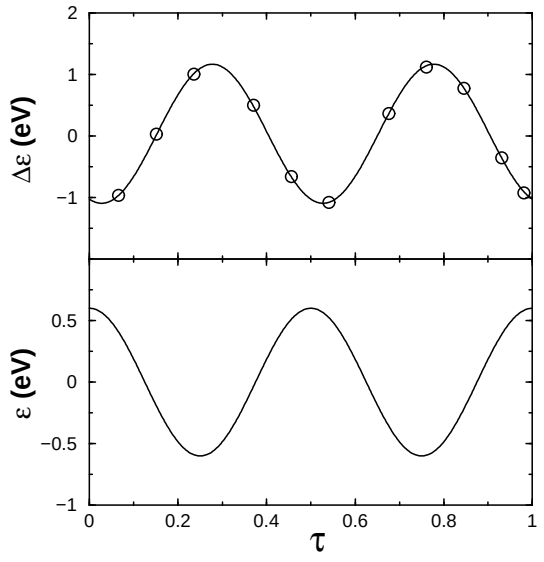

FIG. 3: a) Energy difference between NN hole orbitals as a function of τ. The circles correspond to the computed values, the solid line to the Fourier fit. b) Resulting hole orbital energies, the energy zero have been chosen to be the average value.

The orbital energies are dependant on different parameters. The most important are (i) the amount of delocalization toward the neighboring atoms (strongly affects the kinetic energy), (ii) the electrostatic potential from the rest of the crystal. In the present cas, we have seen that the delocalization of the spin and hole orbitals on the oxygen atoms is nearly constant. The variation of the orbital energy can thus be expected to be induced by the variation of the Madelung potential. Figure 4 reports the variation of the orbital energy differences between NN sites as a function of the related Madelung potential energy differences on the copper sites (centroid of the orbitals). One notice immediately the nearly perfect scaling between the Madelung potential and the orbital energy, thus confirming the above analysis. Let us point out that this scaling does not appear as clearly if one plots the orbital energy differences as a function of the Madelung potential differences, averaged on the four oxygen atoms.

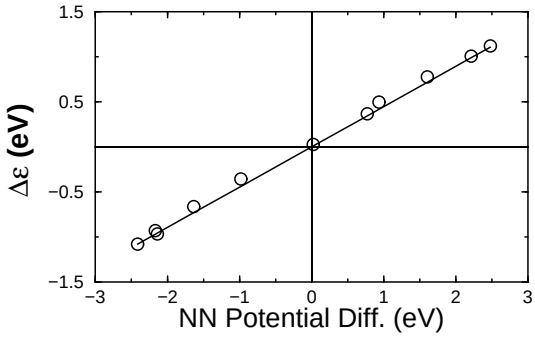

FIG. 4: Orbital energy differences between NN sites as a function of the associated Madelung potential energy differences computed on the orbital centroid (copper sites).

Let us now analyse the origin of such large Madelung potential variations. These modulations can originate from three terms.

- The relative displacement of the ladders and the chain subsystems in the average structure (due to incommensurate c_l and c_c parameters).
- The ladder subsystem modulation.
- The chain subsystem modulation.

Figure 5 reports the Madelung potential differences between NN copper sites taking into account independantly these three effects. One notice immediately that the influence of the incommensurability alone has a nearly negligeable effect on the Madelung potential variations. Indeed, its amplitude is of only 30 meV. One could however have expected it to strongly contribute since the

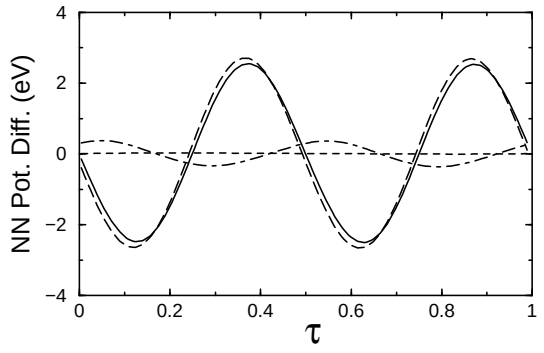

FIG. 5: Madelung potential differences between NN copper sites, dashed : computed only from the average crystallographic structure, dot-dashed : with added ladder modulations, long-dashed : with added chain modulations, solid-line : with both chain and ladder modulations (exact structure).

strontium ions are attached to the ladders and are located close to the chains. The ladder subsystem influence is quite small even if non negligeable, with a range of 0.73 eV. In fact, the origin of the chain potential variations comes mainly from the chain modulation itself. Indeed, it accounts for more than 95% of the potential modulation.

B. The NN hopping and exchange effective integrals

Figure 6 reports the NN effective hopping and exchange integrals as a function of the fourth crystallographic coordinate τ. These integrals have been evaluated both from the two-centers and three-centers fragments. The three-centers fragments used in the calculations have been chosen in successive positions along the chain. Thus, each NN integral appears in two successive fragments yielding independant evaluations. One should first notice that the three independant evaluations of the the NN hopping, t_1, and exchange, J_1, integrals yield the same values, thus validating the second neighbor $t-J+V$ model used in the present work. Indeed, whether other interactions or orbitals would have been of importance, the two-centers and three-centers calculations would have given different evaluations of the integrals so that to compensate the inability for the model to reproduce the low-energy local physics.

The hopping integrals vary over a large range of values, namely from 65meV to 200meV. This can be understood by the fact that the hopping is strongly mediated through the oxygens bridge as soon as the *Cu–O–Cu* angles are different from 90°. Indeed, the *Cu–O–Cu* angle modulations range between 90° and 96°. The exchange integral is, as expected, ferromagnetic. Its amplitude of relative variation is much weaker than the hopping one. Namely, it ranges between 17 meV and 26 meV. This smaller amplitude of the variation is due to the fact that the dominating term is the direct exchange term, responsible for the ferromagnetic character of the integral. The super-exchange term, antiferromagnetic in nature and mediated by the bridging oxygens, is smaller that the direct one. It is anyway responsible for most of the observed exchange modulations through the variation of the *Cu–O–Cu* angle.

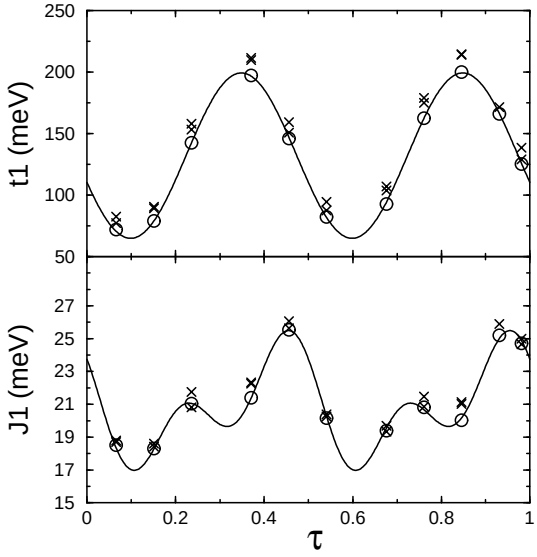

FIG. 6: Nearest-neighbor effective hopping (a) and exchange (b) integrals as a function of τ. The circles correspond to the two-coppers fragment calculations, the cross to the three-coppers calculations and the solid line to the Fourier fit.

C. The NNN hopping and exchange effective integrals

Figure 7 reports the NNN effective hopping and exchange integrals as a function of the fourth crystallographic coordinate τ. The first thing one notices is that the second neighbor hopping integrals are larger in amplitude than the first neighbor ones. Eventhough surprising, because of the large *Cu–Cu* distances ($\simeq 5.4$Å), this large NNN hopping is due to the fact that on the contrary to the NN interactions, the oxygen mediation of the integral is very strong. Indeed, while the NN hole orbitals are nearly orthogonal, the NNN hole orbitals strongly overlap (see figure 2b). The NNN direct exchange term, ferromagnetic in nature, can be considered as negligeable, due to the large copper-copper distance. The NNN exchange is thus dominated by the super-exchange mechanism mediated through the bridging oxygens. It results a weak, antiferromagnetic integral, in agreement with the experimental findings. Indeed, these results are to be compared with the experimental evaluations[2] of the intra-dimer exchange integrals of -11 meV.

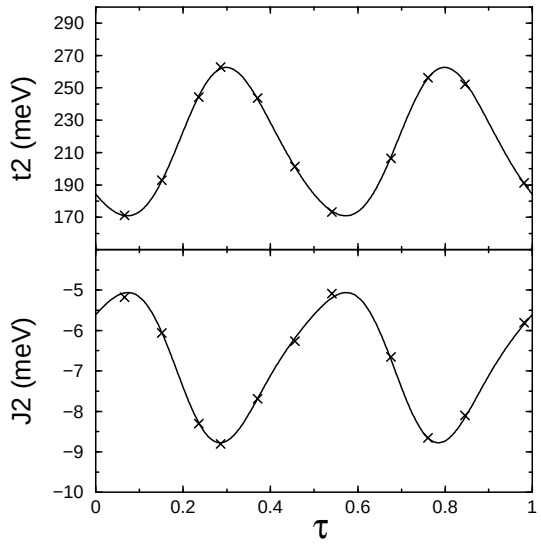

FIG. 7: Next nearest neighbor effective hopping (a) and exchange (b) integrals as a function of τ. Crosses correspond to the computed points, solid line to the Fourier fit.

D. The NN bielectronic repulsion

Figure 8 reports the NN effective repulsion as a function of the fourth crystallographic coordinate τ. The repulsion integral, V, can be evaluated independantly from two successive three-centers fragments. One sees that V is much less sensitive than the other parameters to the structural modulations. Indeed, its variation range accounts for only 19% of its nominal value, 0.66 eV. Let us notice, that the two independant evaluations are again in good agreement.

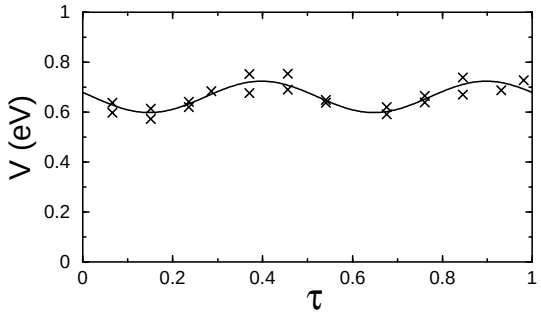

FIG. 8: Nearest neighbor effective bi-electronic repulsion as a function of τ. Crosses correspond to the computed points, solid line to the Fourier fit.

V. FILLING ANALYSIS

As mentioned above, the large orbital energy variations induce a localization of the spins (holes) along the chain. The above model can be used to determine the spins arrangement over a region of the chain. Figure 9 shows the spins localization over 41 consecutive sites. All the holes have been supposed to be localized on the chains since it has been shown in reference[16] that this filling agrees with the experimental data. Indeed, one sees that the following experimentally-observed properties are correctly reproduced : i) the presence of a small proportion of free spins, as seen in magnetic succeptibility measurements, and ii) the formation of second-neighbor dimers separated by two Zhang-Rice singlets, as seen in neutron scattering experiments. Nevertheless, the above fragment represent only a small fraction of the chain and, due to the incommensurate character of the crystallographic structure, there is no warranty that the properties observed on figure 9 are characteristic of the whole chain. In order to validate the present electron localization model, we need to make a study of the filling using the four-dimensional crystallographic representation.

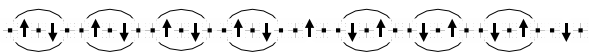

FIG. 9: Localization of the spins (holes) on 41 consecutive sites along the chain.

The aim of the four-dimensional analysis is to partition the whole system (here the chains) into physically pertinents blocks and to detemine (i) the number of different type of blocks, (ii) their relative arrangement and (iii) their rate of existence in the incommensurate structure. For this purpose it is usefull to start with a chosen type of block, expected to be largely represented in the system. In the present case it could be the dimeric units. Then, the model hamiltonian is used to determine the apparition of this type of blocks as a function of the fourth component. The analysis of the remaining sites allows to determine the other types of significant blocks present in the system. Finally, the relative arrangement of the types of blocks can be studied.

As mentioned, we will chose in the present system the dimeric units as starting blocks. These units are composed of five sites, the three sites of the dimer plus the two ZR singlets of the neighboring sites (see figure 10). Let us use the fourth coordinate of the first site (τ_1) as the block reference. If one plots the energy of five consecutive sites as a function of τ_1, a dimeric unit will thus be obtained when the energy of the second and fourth sites are

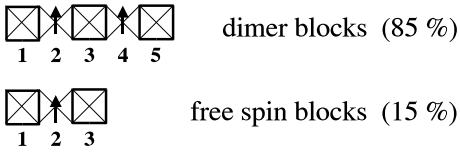

FIG. 10: The different types of spin blocks appearing in the chains. Values in paraentheses refer to the percentage of the chain corresponding to the different types of blocks.

below the Fermi level, while the energy of the first, third and fifth sites are above the Fermi level. Figure 11 shows the orbital energy curves of five consecutive sites as a function of τ_1. Let us notice that, since five sites are represented by a unique value of τ, only one fifth of the $[0,1]$ range is necessary to represent the whole chain. The values of τ_1 for which the five consecutive sites form a dimer are represented in gray. It spans a range of twice 0.085. The proportion of the chain occupied by dimers thus corresponds to five time the above ranges, that is 85%. Finally the number of dimers can be evaluated to 1.70 per f.u., to be compared to 1.47 dimer per f.u. deduced from magnetic succeptibility measurements[2]. Let us now analyse the composition of the remaining 15% of the chain. For this purpose we will determine the number of sites separating two consecutive dimers. If τ_1 is referencing the first dimer (that is $\tau_1 \in [0.068\,;\,0.153] \cup [0.568\,;\,0.653]$) than the reference of the second dimer is given by $\tau_1' = \tau_1 + n(\tau_1)c_c/c_l$, where $n(\tau_1)$ is the smaller integer such that $\tau_1' \in [0.068\,;\,0.153] \cup [0.568\,;\,0.653]$. At this stage three cases can occur.

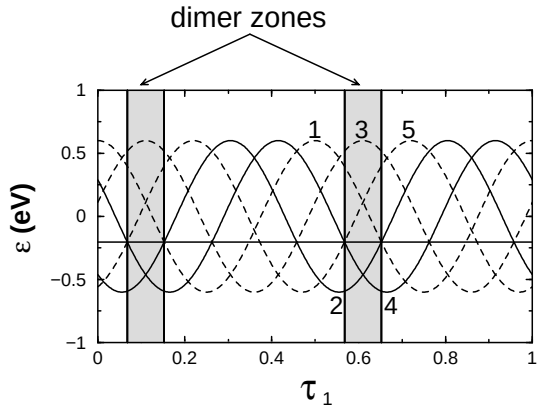

FIG. 11: Orbital energies of five consecutive sites as a function of the fourth coordinate τ_1 of the first one. The horizontal line represent the Fermi level.

1. case. $n(\tau_1) < 5$. In this case, the two successive dimers overlap, in other words there exist physical entities larger than the dimers.

2. case. $n(\tau_1) = 5$. In this case, the two dimers are strictly consecutive along the chain.

3. case. $n(\tau_1) > 5$. In this case, the two successive dimers are separated by one or several other type of blocks of total length : $n(\tau_1) - 5$.

In the present system, only $n = 5$ and $n = 8$ occurs. As stated above the former corresponds to consecutive dimers and the latter to dimers separated by three sites blocks. As for the dimers, we will reference these blocks by the fourth coordinate of their first site, that is $\tau_1 + 5\,c_c/c_l$. The three sites blocks thus span two ranges : $[0.042\,;\,0.068]$ and $[0.542\,;\,0.568]$. Figure 12 represents the three sites blocks and the dimer ranges for $\tau_1 < 0.5$. In each region, the orbital energy of each site of the block has been represented. One sees immediately that the three sites blocks are formed by one spin surrounded by two ZR singlets. Such a configuration can be assossiated with free spins since the nearest neighbor spin is two ZR singlets afar. Let us notice that three times the free spins ranges yields 0.15, that is the total missing part of the chain. The number of free spins can be now easily evaluated to 0.5 per f.u., to be compared to 0.55 free spins per f.u. obtained from the magnetic succeptibility experiments.

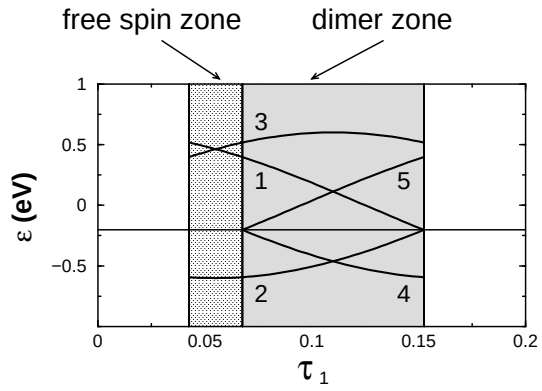

FIG. 12: Orbital energy of block sites for the two different type of blocks given as a function of the fourth coordinate τ_1 of the first site of each block. The horizontal line represent the Fermi level.

A further analysis of the figure 11 shows that the dimers are arranged in clusters of three or four dimers separated by a free spin. It can be evaluated that 54% of the dimers form three-dimers clusters while 46% form four-dimers clusters.

VI. CONCLUSION

To summarize the present results, we have determined a second neighbor $t - J + V$ model for the incommensurate chain subsystem of the $Sr_{14}Cu_{24}O_{41}$ compound. The model parameters have been determined using accurate ab initio calculations on a series of embedded clusters along the chain. In order to obtain a complete model as a function of the incommensurate modulation, the ab initio results have been extrapolated using a Fourier analysis. The resulting model is thus independant of any periodic approximation since it is given as a continuous function of the fourth crystallographic coordinate τ, which describes the incommensurate modulations along the chain.

It is noticeable that, unlike what is currently assumed in the litterature, the various parameters of the model, except for the first neighbor bi-electronic repulsion, strongly vary as a function of the structural incommensurate modulations. In fact, these variations are so large that they determine the physics of the system. In

particular, the orbital energies vary over a surprisingly large range, and thus dominate the low energy physics through a strong localization of the electron (resp. holes) over the low (resp. high) energy sites. It has been identified that the orbital energy modulation originates in the Madelung potential modulation associated with the chain distorsions. Indeed, the orbital energies are shown to be proportional to the electrostatic potential on the copper centers, all other effects being at least an order of magnitude weaker. Another noticeable point is the weak contribution of the ladder subsystem to the electrostatic potential modulations, despite of its incommensurate translation vector with the chain subsystem.

The analysis of the model as a function of the fourth crystallographic coordinate τ allowed us to show that the chain ground state can be entirely described only by second-neighbor dimers and free spins. The dimers are arranged in clusters of three or four units separated by a free spin. We retrieve in our calculation the proportion of free spins obtained from magnetic succeptibility measurements. We have also been able to show that the holes do not localize on the copper atoms but rather on the surrounding oxygen p orbitals, thus confirming the hypothesis of the presence of Zhang-Rice singlets. Three types of Zhang-Rice singlets can be identified in our calculations, namely the intra-dimer ones, and two types of inter-dimer ones : those neighboring dimers and those neighboring free spins. This result is to be put in perspective with the copper RMN experiments[4] that sees a splitting of the inter-dimer Zhang-Rice singlets signal at low temperatures. It would be interresting to quantify the relative weight of the two signals in order to check our predicted ratio of 3.4.

Acknowledgment : the authors thank Dr. J. Etrillard for providing us with the neutron crystallographic structures as well as for helpfull discussions, Dr. D. Maynau for providing us with the CASDI suite of programs, Dr. Ph. Sciau for introducing us with the four-dimensional crystallographic conventions.

[1] M. McCarron et al., Mater Res. Bull. **23**, 1355 (1988)
[2] S.A. Carter *et al.*, Phys. Rev. Lett. **77**, 1378 (1996).
[3] R.S. Eccleston, M. Azuma and M. Takano, Phys. Rev. **B 53**, 14721 (1996) ; M. Matsuda *et al.*, Phys. Rev. **B 54**, 12199 (1996).
[4] K. Magishi *et al.*, Phys. Rev. **B 57**, 11533 (1998).
[5] S. Tsuji *et al.*, J. Phys. Soc. Jap. **65**, 3474 (1996) ; K.Kumagai *et al.*, Phys. Rev. Lett. **78**, 1992 (1997).
[6] M. Takigawa *et al.*, Phys. Rev. **B 57**, 1124 (1998).
[7] R.S. Eccleston *et al.*, Phys. Rev. Lett. **81**, 1702 (1998).
[8] U. Ammerahl *et al.*, Phys. Rev. **B 62**, 8630 (2000).
[9] M. Kato, K. Shiota and Y Koike, Physica C **258**, 284 (1996).
[10] F. C. Zhang and T. M. Rice, Phys. Rev. **B 37**, 3759 (1988).
[11] N. Nücker *et al.*, Phys. Rev. **B 62**, 14384 (2000).
[12] D.E. Cox, I. Iglesiais, K. Hirota, G. Shirane, M. Matsuda, N. Motoyama, H. Eisaki and S. Uchida, Phys. Rev. **B 57**, 10750 (1998).
[13] L.P. Regnault *et al.*, Phys. Rev. **B 59**, 1055 (1999) ; M. Matsuda *et al.*, Phys. Rev. **B 59**, 1060 (1999).
[14] C. K. Majumdar and D. K. Gosh, J. Math. Phys **10** 1399 (1969).
[15] F. D. M. Haldane, Phys. Rev. **B 25** 4925 (1982).
[16] A. Gellé and M.-B. Lepetit, Phys. Rev. Letters, in press.
[17] M.-B. Lepetit, *Recent Research Develepments in Quantum Chemistry*, p. 143, Vol. 3, Transworld research Network (2002).
[18] N. W. Winter, R. M. Pitzer and D. K. Temple, *J. Chem. Phys.* **86**, 3549 (1987).
[19] J. Miralles, J. P. Daudey and R. Caballol, Chem. Phys. Lett. **198**, 555 (1992) ; V. M. García *et al.*, Chem. Phys. Lett. **238**, 222 (1995) ; V. M. García, M. Reguero and R. Caballol, Theor. Chem. Acc. **98**, 50 (1997).
[20] D. Muñoz, F. Illas and I. de P.R. Moreira, Phys. Rev. Letters **84**, 1579 (2000) ; D. Muñoz, I. de P.R. Moreira and F. Illas, Phys. Rev.**B 65**, 224521 (2002).
[21] N. Suaud and M.-B. Lepetit, Phys. Rev. **B 62** 402 (2000) ; N. Suaud and M.-B. Lepetit, Phys. Rev. Letters **88**, 056405 (2002).
[22] M. Isobe *et al.*, Phys. Rev. **B 62**, 11667 (2000) ; J. Etrillard *et al.*, Physica C, in press.
[23] H. M. Evjen, **Phys. Rev. 39**, 675 (1932).
[24] A. Gellé and M.-B. Lepetit, unpublished.
[25] P.M. de Wolff, Acta Cryst. A **30**, 777 (1974).
[26] M. Isobe, Y. Uchida, and E. Takayama-Muromachi, Phys. Rev. **B 59**, 8703 (1999).